JAST, Vol. 4, No. 3, pp 1–11

JAST
Journal of Aerospace Science and Technology

Improved Mathematical Model for Helicopter Flight Dynamics Applications

F. Saghafi[1], F. Shahmiri[2]

This paper is concerned with the mathematical model development issues necessary for better prediction of dynamic responses of articulated rotor helicopters. The methodology is laid out based on mathematical model development for articulated rotor helicopters, using the theories of aeroelastisity, finite element and the time domain compressible unsteady aerodynamics. The helicopter is represented by a set of coupled nonlinear partial differential equations for the main rotor within nonlinear first order ordinary differential equations representation, describing the dynamics of the rest of the helicopter. The complexity of the formulation imposes the use of numerical solution techniques for dynamic response calculations. The validation is performed by comparing simulated responses to flight test data for a known configuration. The results show improvement in dynamic response prediction of both on-axis and cross-coupled responses of helicopter to pilot inputs.

NOMENCLATURE

a	Speed of sound
A	Blade section area
a_{ij}	Matrix array
c	Length of the blade chord
C_l, C_d, C_m	Lift, drag and pitching moment coefficients of airfoil section
C_{d0}, C_n	Skin friction drag coefficient, normal force coefficient
C_T	Main rotor thrust coefficient
e	Hinge offset of main rotor blade
x	Vector of the Unsteady aerodynamic states
x_{ac}	Aerodynamic center
x_{ea}	Elastic center/shear center
ψ_b	Blade azimuth angle
u_b, v_b, w_b	Axial, Lagwise and flapwise elastic deflection of a point on the blade
ϕ_b	Elastic rotation/twist
α, β	Fuselage angle of attack, sideslip angle
α_m	Mean angle of attack of airfoil section
θ_{tw}	Blade built-in-twist
ρ	Blade mass density
σ	Main rotor solidity
μ	Advanced ratio
$(..)_A$	Aerodynamic loads index
$(..)_I$	Inertial loads index
$(..)_S$	Structural loads index
$(..)^{\cdot}$	Partial derivative with respect to time
$(..)^{\cdot\cdot}$	Second partial derivative with respect to time
$(..)^T$	Transpose
$(..)_{,x}$	Partial derivative with respect to

1. *Associate Professor, Dept. of Aerospace Eng., Sharif Univ. of Tech., Email: saghafi@sharif.ir.*
2. *Ph.D Candidate, Dept. of Aerospace Eng., Sharif Univ. of Tech., Email: farid_shahmiri@yahoo.co.uk.*

INTRODUCTION

In recent years, the need for more reliable designed helicopters has caused an increasing interest in improving the accuracy of flight dynamics mathematical models of helicopters. This has led to more advanced modeling of the rotor system, both from the dynamics and the aerodynamics point of view. Particular attention has been paid to the long-term problem of off-axis response prediction errors in flight dynamics modeling, especially in pitch and roll cross coupling. Until recently, the predictions of the off-axis response (*e.g.*,

the pitch response to a lateral cyclic pitch input) were inaccurate compared to the results of flight tests.

The first major contribution to the understanding of the off-axis response problem has been made by Rosen and Isser [1, 2], attributing the prediction errors to the incorrect modeling of the geometry of the main rotor wake during pitch and roll maneuvers. Pitch and roll motion reduce the spacing of the wake vortices on one side of the rotor disk, and increase it on the opposite side. This change in wake geometry modifies the inflow distribution at the rotor disk, causes changes in blade flapping, and in turn changes in pitch and roll moments. Taking into account these geometry changes through a specially developed prescribed wake model improved the prediction of cross-coupling pitch and roll derivatives for the UH-60 and the AH-64.

Following Rosen and Isser's work, other researchers have developed aerodynamic models that capture the inflow changes due to a maneuver using correction coefficients. Keller [3] and Arnold *et. al.* [4] have developed an extended momentum theory that contains simple additional inflow terms proportional to pitch and roll rates. The additional terms consist of correction coefficients, the numerical values are determined based on a simplified vortex wake analysis. Slight improvements were obtained for the prediction of the off-axis response of the UH-60. Basset [5] who used a dynamic vortex wake model has modeled the wake geometry changes due to a maneuver. In this model, the vortex rings represent the wake. Substantial improvements in the prediction of the hover off-axis response for the BO-105 were obtained.

Von Gräunhagen [6] has suggested a completely different explanation for the discrepancies of off-axis predictions by a virtual inertia effect associated with the swirl in the rotor wake. This results in simple correction terms that can be added to a dynamic inflow theory. Some improvements in off-axis predictions for a BO- 105 were reported.

All previous studies have tried to improve the prediction of the off-axis response through theoretical models. Mansur and Tischler [7] have proposed a different approach by the use of corrected lift and drag coefficients of the blade airfoils obtained from a first-order filter. The time constant is chosen in terms of an aerodynamic phase lag. This phase lag is also determined from flight test data by using system identification techniques.

Finally, the alternative approaches are offered through implementation of refined free wake models. The models that can capture the wake structure due to pitch and roll rates has been recently developed by Celi *et. al.* [8-14]. Some simplifications in the assumptions, namely the structure of vortex filaments, vortex core size, velocity profile through the vortex, initial strength and diffusion of the velocities, and discretization of vortex wake are still observed in this modeling, and hence, these are led to discrepancy problem relative to flight test data.

In the present research, response improvement is acquired through modifying the helicopter flight dynamics mathematical model by incorporating the generalized, three dimensional, compressible, unsteady aerodynamics modeling in the time domain. Although this unsteady aerodynamic model has a challenge from the viewpoint of the computational expenses, it has several advantages when it appends to the rest of helicopter mathematical model. In the following, a gradual manner for constructing the mathematical model development is firstly presented, which is then followed by a representation of the results and discussions on their validities and improvements.

MAIN ROTOR EQUATIONS OF MOTION

This section is composed of a brief description of the mathematical model of the main rotor system. The main rotor blades are modeled as flexible beams experiencing coupled flap, lag, and torsional motion. The blade equations of motion are derived from combining the main rotor inertial, aerodynamic, and structural loads through the calculation of the absolute acceleration and velocity vector of a generic point on the blade elastic axis with respect to inertial coordinate system. The result is a set of nonlinear-coupled partial differential equations with periodic coefficients in the undeformed coordinate system. These equations are ultimately transformed into a system of nonlinear-coupled ordinary differential equations using the finite element discretization based on the Galerkin method of weighted residuals [15]. Figure 1 illustrates the element and the corresponding nodal degrees of freedom, which is considered for the current study. According to the figure, the total number of degrees of freedom for a blade finite element is eleven.

Hence, the total number of the blade degrees of freedom for a whole blade with N_e finite elements

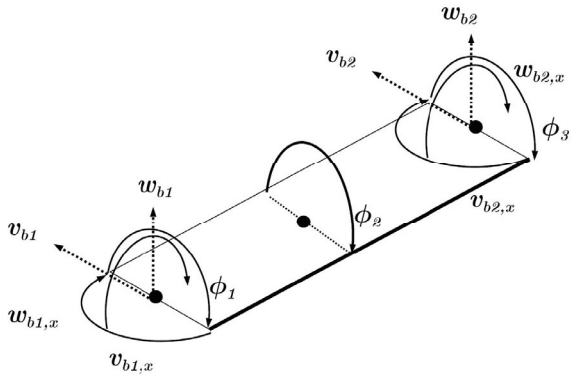

Figure 1. Schematic of the blade element degrees of freedom.

corresponds to $n = 6\,N_e + 5$. The degrees of freedom are ordered as follows to form the vector of nodal displacements, y_n:

$$y_n = \big(v_{b1}\ v_{b1,x}\ \cdots\ v_{b(N_e+1)}\ v_{b(N_e+1),x}\ w_{b1}\ w_{b1,x}\ \cdots\ w_{b(N_e+1)}\ w_{b(N_e+1),x}\ \phi_{b1}\ \cdots\ \phi_{b(2N_e+1)}\big)^T \tag{1}$$

This total is reduced by applying of the boundary conditions. For an articulated rotor, the total is reduced by three, since v_{b1}, w_{b1} and ϕ_{b1} are zero for the first element, corresponding to the location of the hinge. For making a reduction in either the blade elements nodal degrees of freedom or the computational expenses, the modal coordinate transformation is also required. This means that the vector of finite element degrees of freedom y_n is written as the product of a modal coordinate transformation matrix $[V]$ and a vector q of modal coefficients as:

$$y_n = [V]\ q \tag{2}$$

The nonlinear-coupled second order ordinary differential equations of the main rotor in the modal space are finally generated as:

$$\ddot{q}_{i_b}^{i_m}(\psi_b) = f\left(\dot{q}_{i_b}^{i_m}, q_{i_b}^{i_m}\right) \qquad i_b = 1, ..., N_b = 4\,,\ \ i_m = 1, ..., N_m = 6 \tag{3}$$

where, N_b and N_m are in turn, the total number main rotor blade and the number of selected modes for modal coordinate transformation. The main rotor equations are ultimately appended to the rest of the helicopter mathematical model, which is defined as:

$$\dot{y} = F(y, u; t) \tag{4}$$

where, y is the state vector, u the control vector and t is time. In other words:

$$y = \big(u\ v\ w\ p\ q\ r\ \phi\ \theta\ \psi\ q_1^1\ q_2^1\ q_3^1\ q_4^1\ \dot{q}_1^1 \dot{q}_2^1\ \dot{q}_3^1\ \dot{q}_4^1 \cdots\ q_1^{Nm}\ q_2^{Nm}\ q_3^{Nm}\ q_4^{Nm}\ \dot{q}_1^{Nm}\ \dot{q}_2^{Nm}\ \dot{q}_3^{Nm}\ \dot{q}_4^{Nm}\ \lambda_0\ \lambda_{1c}\ \lambda_{1s}\ v_{tr}\ \Omega\ x_1\ x_2\ x_3\ \cdots\ x_{8\times Np\times Nb}\big)^T \tag{5}$$

and

$$u = (\theta_0\ \ \theta_{1c}\ \ \theta_{1s}\ \ \theta_{0tr})^T \tag{6}$$

where u, v, w are translational velocity components of the body in the body fixed coordinate system, p, q, r the angular velocity of the body in the body coordinate system, ϕ, θ, ψ Euler angles, q modal coefficient terms, $\lambda_0, \lambda_{1c}, \lambda_{1s}$ uniform, cosine and sine inflow components respectively, Ω the rotor speed, v_{tr} uniform inflow of the tail rotor, N_p the number of unsteady points on the blade span, and where x's are the unsteady aerodynamic states.

In Eq. (6), the control vector also consists of the main rotor collective pitch, the lateral, longitudinal cyclic pitch, and the tail rotor collective respectively. Because the coupled rotor-fuselage-inflow equations of motion have the state derivatives appearing on the right hand side of the Eq. (4), this equation is rewritten as:

$$\dot{y}_c = F_c(\dot{y}, y, u; t) \tag{7}$$

where, $\dot{y}_c$ is the inertial coupling vector, which contains all the state derivatives appearing on the right hand side of Eq. (4).

$$\dot{y}_c = \left(\dot{u}\ \dot{v}\ \dot{w}\ \dot{p}\ \dot{q}\ \dot{r}\ \dot{\Omega}\ \ddot{q}_1^1\ \cdots\ \ddot{q}_4^1\ \ddot{q}_1^{Nm}\ \cdots\ \ddot{q}_4^{Nm}\right)^T \tag{8}$$

The Eq. (7) can be arranged as follow:

$$\dot{y}_c = [E]\,\dot{y}_c + F_k(y, u; t) \tag{9}$$

Re-arranging Eq. (9) and express it as follow:

$$\begin{bmatrix}\dot{y}_{fus}\\ \dot{y}_{mr}\end{bmatrix}_c = \begin{bmatrix}E_{11} & E_{12}\\ E_{21} & E_{22}\end{bmatrix}\begin{bmatrix}\dot{y}_{fus}\\ \dot{y}_{mr}\end{bmatrix}_c + F_{mr} + F_{tr} + F_{fus} \tag{10}$$

where

$$\dot{y}_{fus} = (\dot{u}\ \dot{v}\ \dot{w}\ \dot{p}\ \dot{q}\ \dot{r})^T \tag{11}$$

and

$$\dot{y}_{mr} = \left(\dot{\Omega}\ \ddot{q}_1^1\ \ddot{q}_2^1\ \ddot{q}_3^1\ \ddot{q}_4^1\ \cdots\ \ddot{q}_1^{Nm}\ \ddot{q}_2^{Nm}\ \ddot{q}_3^{Nm}\ \ddot{q}_4^{Nm}\right)^T \tag{12}$$

In Eq. (10), $[E_{11}\,\dot{y}_{fus}]$ is the inertial acceleration due to the fuselage, $[E_{12}\,\dot{y}_{mr}]$ is the inertial acceleration due to the main rotor, F_{mr} is acceleration contributed by the main rotor excluding the inertial coupling term, F_{tr} is the acceleration contributed by the tail rotor, and F_{fus} is the acceleration contributed by the fuselage, the horizontal, and the vertical surfaces [15].

Main Rotor Inertial Loads

A basic way for the calculation of the inertia force and moments is to find the absolute velocity of a point on the elastic axis of the blade, which is the derivative of the position vector of a point on the elastic axis relative to the inertial coordinate system, R. The acceleration

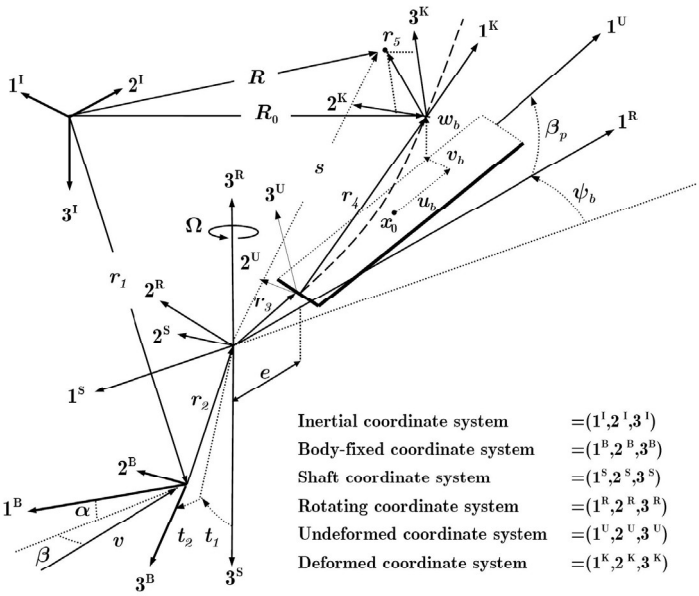

Figure 2. Schematic of the helicopter coordinate systems.

vector is given by [15]:

$$
\begin{aligned}
(P_I^2 R)^U = {} & (P_I^2 r_1)^U \\
& + (P_B^2 r_2)^U + (P_B(w_{IB} \times r_2))^U \\
& + (w_{IB} \times (P_B r_2 + w_{IB} \times r_2))^U \\
& + (P_U^2 r_3)^U + (P_U(w_{IU} \times r_3))^U \\
& + (w_{IU} \times (P_U r_3 + w_{IU} \times r_3))^U \\
& + (P_U^2 r_4)^U + (P_U(w_{IU} \times r_4))^U \\
& + (w_{IU} \times (P_U r_4 + w_{IU} \times r_4))^U \\
& + (P_K^2 r_5)^U + (P_K(w_{IK} \times r_5))^U \\
& + (w_{IK} \times (P_K r_5 + w_{IK} \times r_5))^U
\end{aligned} \tag{13}
$$

where the operator P is given by:

$$
P^2 = \left(\frac{\partial^2}{\partial t^2}\right), \qquad P = \left(\frac{\partial}{\partial t}\right) \tag{14}
$$

In Eq. (13), r_i is the position vector; w_{ij} is the angular velocity of the j-coordinate system with respect to the i-coordinate system; the superscript $(..)^i$ is used to indicate that the quantity is defined in the i-coordinate system, the subscripts of the P operator indicate the position from which the observer looks at the vector. Figure 2 illustrates the position vectors and the corresponding coordinate systems.

The inertial loads per unit span in the undeformed coordinate system are finally determined by integration of Eq. (13) as:

$$
\begin{aligned}
(F_I)^U &= -\iint_A \rho \left(P_I^2 R\right)^U dA \\
(M_I)^U &= -\iint_A \rho \left(r_5 \times P_I^2 R\right)^U dA
\end{aligned} \tag{15}
$$

Equation (15), based on the inertial coupling vector which is defined in Eq. (9), can be arranged as;

$$
\begin{aligned}
(F_I)^U &= [E_{F_I}]\, \dot{y}_c + F_{F_I}(y;t) \\
(M_I)^U &= [E_{M_I}]\, \dot{y}_c + F_{M_I}(y;t)
\end{aligned} \tag{16}
$$

Structural Modeling of the Rotor Blade

In this section, the structural formulation for the rotor blade is briefly described. The formulation is essentially based on coupled flap-lag bending, rigid pitch, and elastic torsion motion of a blade. The blade is assumed to be a slender rod made of the linearly isotropic material, and that the out of plane warping and strains within the cross section are neglected. The derivations are based on the Bernoulli-Euler beam hypothesis such that it is restricted to the case of the moderate deflections. The final stage of this analysis is converged to the stress-force relations in the K-coordinate system as follows:

$$
\begin{aligned}
(F_S)^K &= \iint_A (\sigma)^K dA \\
(M_S)^K &= \iint_A (r_5 \times \sigma)^K dA
\end{aligned} \tag{17}
$$

where

$$(\sigma)^K = (\sigma_{xx} \ \ \tau_{xy} \ \ \tau_{xz})^T$$
$$(r_5)^K = (0 \ \ y_0 \ \ z_0)^T \tag{18}$$

The stress-strain relations are obtained as:

$$\varepsilon_{xx} = E\sigma_{xx} = \frac{1}{2}(G_X \cdot G_X - 1)$$
$$\varepsilon_{xy} = 2G\tau_{xx} = \frac{1}{2}(G_X \cdot G_Y)$$
$$\varepsilon_{xz} = 2G\tau_{xx} = \frac{1}{2}(G_X \cdot G_Z) \tag{19}$$

where, the base vectors of the deformed section at the specified point are obtained as:

$$G_X = \frac{\partial s}{\partial x}, \qquad G_Y = \frac{\partial s}{\partial y}, \qquad G_Z = \frac{\partial s}{\partial z} \tag{20}$$

As shown in Figure 2, $s = r_3 + r_4 + r_5$ is the position vector of the point on the deformed blade section relative to hub center.

Finally, the structural loads in the undeformed coordinate system are obtained through implementing the relevant transformation matrix c_k^u. This is because of the fact that the main rotor equations of motion are eventually presented in the undeformed coordinate system [15].

$$(F_S)^U = C_K^U (F_S)^K$$
$$(M_S)^U = C_K^U (M_S)^K \tag{21}$$

Main Rotor Aerodynamic Loads

The way for calculating the main rotor air-loads is to determine the total velocity vector of a point on the blade elastic axis, R_0 in the undeformed coordinate system as:

$$(v_T)^U = (P_I r_1)^U + (P_B r_2 + w_{IB} \times r_2)^U + (P_S r_3 + w_{IS} \times r_3)^U + (P_U r_2 + w_{IU} \times r_4)^U + C_R^U C_S^R C_{TPP}^S (\lambda)^{TPP} \tag{22}$$

where the last term in the right hand side, $(\lambda)^{TPP} = (0 \ 0 \ \lambda_i)^T$ is the contribution of the induced velocity by the rotor wake, which is known in the tip path plane coordinate system [13]. Figure 3 illustrates the tip path plane coordinate system of the main rotor.

The total local velocity components, Eq. (22), in the blade sectional aerodynamic coordinate system $(1^L, 2^L, 3^L)$, can be expressed as:

$$(v)^L = (v_T \ v_P \ v_R)^T = C_U^L (v_T)^U \tag{23}$$

Finally, the components of force and moment at 0.25 chord are obtained as:

$$f_T = \frac{1}{2}\rho_{air} c \, v \, (C_d \, v_T - C_l \cos\beta_b \, v_P)$$
$$f_P = \frac{1}{2}\rho_{air} c \, v \, (C_l \, \sec\beta_b \, v_T + C_d \, v_P)$$
$$f_R = \frac{1}{2}\rho_{air} c \, v \, \left(C_d - C_l \, v_T^{-1} v_P \cos\beta_b\right) v_R \tag{24}$$

and

$$(m_R)^L = \frac{1}{2} \, \rho_{air} \, c^2 \, v \, (C_m \, v_T \sec\beta_b + f_P \, (x_{ac} - x_{ea})) \tag{25}$$

where

$$v = \sqrt{v_T^2 + v_P^2 + v_R^2}, \qquad \beta_b = \cos^{-1}\left(\frac{v_T}{\sqrt{v_T^2 + v_R^2}}\right) \tag{26}$$

In this work, the aerodynamic coefficients $c_l(t)$, $c_d(t)$ and $c_m(t)$ are assumed to be time dependent and are thus obtained as follows [16]:

$$C_l(t) = (C_n(t) - C_d(t) \sin\alpha_Y) / \cos\alpha_Y$$
$$C_d(t) = C_{d0} + C_n(t) \sin\alpha_Y \tag{27}$$

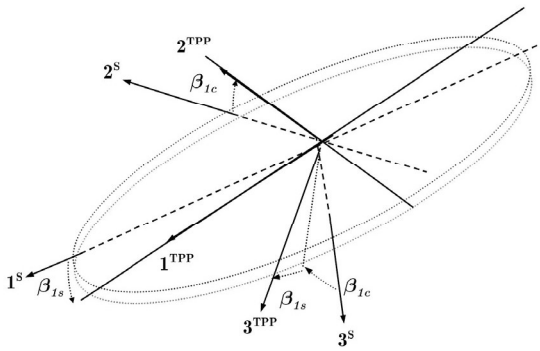

Figure 3. Schematic of the tip path plane coordinate system.

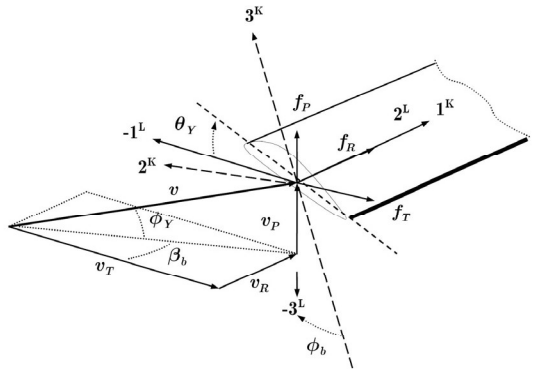

Figure 4. Schematic of the blade angle of attack.

where

$$\tan\alpha_Y = \frac{(v_T\,\tan\theta_b + v_P)\,\sqrt{v_T^2+v_R^2}}{v_T^2+v_R^2-v_P\,v_T\,\tan\theta_b} \tag{28}$$

and

$$\theta_Y = \theta_0 + \theta_{1c}\cos\psi_b + \theta_{1s}\sin\psi_b + \theta_{tw} + \phi_b \tag{29}$$

The unsteady aerodynamic coefficients are obtained based on the fundamental principle that the flow can be linearized about the mean value of angle of attack α_m and pitch rate $q_Y = \dot{\theta}_Y$.

$$\begin{pmatrix}\delta C_n\\ \delta C_m\end{pmatrix} = \begin{pmatrix}C_{n\alpha} & C_{nq}\\ C_{m\alpha} & C_{mq}\end{pmatrix}_{\substack{\alpha_Y=\alpha_m\\ q_Y=q_m}} \begin{pmatrix}\delta\alpha_Y\\ \delta q_Y\end{pmatrix}$$

$$\equiv \left[\begin{pmatrix}C_{n\alpha} & C_{nq}\\ C_{m\alpha} & C_{mq}\end{pmatrix}^{c} + \begin{pmatrix}C_{n\alpha} & C_{nq}\\ C_{m\alpha} & C_{mq}\end{pmatrix}^{nc}\right]_{\substack{\alpha_Y=\alpha_m\\ q_Y=q_m}} \begin{pmatrix}\delta\alpha_Y\\ \delta q_Y\end{pmatrix} \tag{30}$$

where the superscripts c and nc is used to indicate the circulatory and non-circulatory aerodynamic loads respectively.

The circulatory part is the contribution of shed vortices that generates time lag effects in aerodynamic system, and the non-circulatory loads is due to pressure wave propagation once the input is applied. Eq. (30) can be expressed by the extended indicial response theory for subsonic compressible flow as follows:

$$\begin{pmatrix}\delta C_n\\ \delta C_m\end{pmatrix} = \begin{pmatrix}\delta\alpha_Y\\ \delta q_Y\end{pmatrix}$$

$$\left[\begin{pmatrix}a^* & b^*\\ c^* & d^*\end{pmatrix}_{\substack{\alpha_b=\alpha_m\\ q_b=q_m}} + \begin{pmatrix}e^* & \frac{1}{M}e^{-\frac{\left(\frac{2vt}{c}\right)}{T_2}}\\ f^* & -\frac{7}{12M}e^{-\frac{\left(\frac{2vt}{c}\right)}{T_4}}\end{pmatrix}^{nc}_{\substack{\alpha_Y=\alpha_m\\ q_Y=q_m}}\right]$$

$$a^* = \frac{2\pi}{\beta}\left(1-\sum_{i=1}^{2}A_i e^{-b_i\beta^2\frac{2vt}{c}}\right)$$

$$b^* = \frac{\pi}{\beta}\left(1-\sum_{i=1}^{2}A_i e^{-b_i\beta^2\frac{2vt}{c}}\right)$$

$$c^* = \frac{2\pi}{\beta}(0.25-x_{ac})\left(1-\sum_{i=1}^{2}A_i e^{-b_i\beta^2\frac{2vt}{c}}\right)$$

$$d^* = -\frac{\pi}{8\beta}\left(1-e^{-b_5\beta^2\frac{2vt}{c}}\right)$$

$$e^* = \frac{4}{M}e^{-\frac{\left(\frac{2vt}{c}\right)}{T_1}}$$

$$f^* = -\frac{1}{M}\left(A_3 e^{-\frac{\left(\frac{2vt}{c}\right)}{b_3T_3}} + A_4 e^{-\frac{\left(\frac{2vt}{c}\right)}{b_4T_3}}\right) \tag{31}$$

By re-arranging Eq. (31), the state-space form is obtained as follows [16]:

$$\dot{x} = [A]\,x + [B]\,u$$

$$y = [C]\,x + [D]\,u \tag{32}$$

where x is the state vector, u is the input vector, and y is the output vector of the aerodynamic system.

$$\dot{x} = (x_1\ x_2\ x_3\ ...\ x_8)^T$$

$$u = (\delta\alpha_Y\ \ \delta q_Y)^T$$

$$y = (\delta C_n\ \ \delta C_m)^T \tag{33}$$

The unsteady aerodynamic matrices are written as:

$$[A] = \begin{bmatrix} a^{**} & 0 & 0 & 0 & 0 & 0 & 0 & 0\\ 0 & b^{**} & 0 & 0 & 0 & 0 & 0 & 0\\ 0 & 0 & -\frac{a}{cT_1} & 0 & 0 & 0 & 0 & 0\\ 0 & 0 & 0 & -\frac{a}{cT_2} & 0 & 0 & 0 & 0\\ 0 & 0 & 0 & 0 & -\frac{a}{cb_5T_3} & 0 & 0 & 0\\ 0 & 0 & 0 & 0 & 0 & c^{**} & 0 & 0\\ 0 & 0 & 0 & 0 & 0 & 0 & d^{**} & 0\\ 0 & 0 & 0 & 0 & 0 & 0 & 0 & e^{**} \end{bmatrix}$$

$$a^{**} = -\left(\frac{2v}{c}\right)\beta^2 b_1\,, \qquad b^{**} = -\left(\frac{2v}{c}\right)\beta^2 b_2$$

$$c^{**} = -\frac{c}{b_3T_4\,a}\,,\ \ d^{**} = -\left(\frac{2v}{c}\right)\beta^2 b_5\,,\ \ e^{**} = -\frac{a}{c\,b_4T_4} \tag{34}$$

$$[B] = \begin{bmatrix} 1 & 1 & 1 & 0 & 1 & 1 & 0 & 0\\ 0.5 & 0.5 & 0 & 1 & 0 & 0 & 1 & 1 \end{bmatrix}^T \tag{35}$$

$$[C] = \begin{bmatrix} m^* & n^* & o^* & \frac{a_{44}}{M} & 0 & 0 & 0 & 0\\ 0 & 0 & 0 & 0 & -\frac{A_3a_{55}}{M} & -\frac{A_4a_{66}}{M} & p^* & q^* \end{bmatrix}^T$$

$$m^* = 2\pi\left(\frac{2v}{c}\right)\beta A_1 b_1\,, \quad n^* = 2\pi\left(\frac{2v}{c}\right)\beta A_2 b_2$$

$$o^* = \frac{4a_{33}}{M}\,,\ \ p^* = -\frac{\pi}{16}\left(\frac{2v}{c}\right)\beta\,,\ \ q^* = -\frac{7\pi a_{88}}{12M} \tag{36}$$

and

$$[D] = \begin{bmatrix} \frac{4}{M} & -\frac{1}{M}\\ -\frac{1}{M} & -\frac{7}{12M} \end{bmatrix} \tag{37}$$

where

$$\beta = \sqrt{1-M^2} \tag{38}$$

The non-circulatory time constants in Eq. (33) and (34) are equaled to:

$$T_1 = 4M\left[2(1-M) + 2\pi\beta M^2 (A_1 b_1 + A_2 b_2)\right]^{-1}$$

$$T_2 = 2M\left[(1-M) + 2\pi\beta M^2 (A_1 b_1 + A_2 b_2)\right]^{-1}$$

$$T_3 = (A_3 b_4 + A_4 b_3)\left[b_3 b_4 (1-M)\right]^{-1}$$

$$T_4 = 14M\left[15(1-M) + 3\pi\beta M^2 b_5\right]^{-1} \qquad (39)$$

The circulatory constants A_n and b_n are taken from [16].

The unsteady aerodynamic loads is challenged by the computational expenses. This model adds eight states to the overall size of the helicopter model for each point at which the aerodynamic loads are estimated 8-point Gaussian integration. Therefore, it is costly to perform it for the whole of the Gauss points on the blade. Thus, in this case, it is important to be able to calculate the unsteady aerodynamics states only at a reduced set of points and interpolate the results to the Gauss points prior to integration.

The interpolation may occur at any of a number of steps of the calculation of the unsteady aerodynamic loads. For instance, after integrating the unsteady aerodynamic state, $\dot{x}$, for the selected spanwise points, the generated states x have to be interpolated to provide values at each of the Gauss points locations. In other words, it is possible to do calculations up to the time of determination of the states, $\dot{x}$, at the selected sample points, and then interpolate them into the Gauss points prior to integration. The latter procedure has been implemented in this study because it gives the minimum computational cost and it is found that the sensitivity of aerodynamic loads to the values of the unsteady aerodynamic states is very high. The interpolation procedure implemented here is based on a Cubic Spline [17].

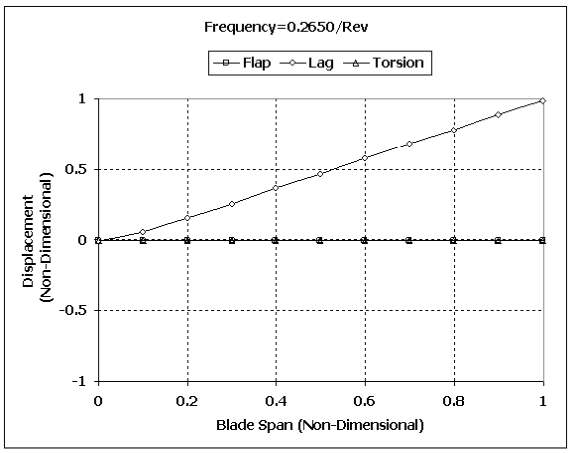

Figure 5. Schematic of the 1st natural blade mode.

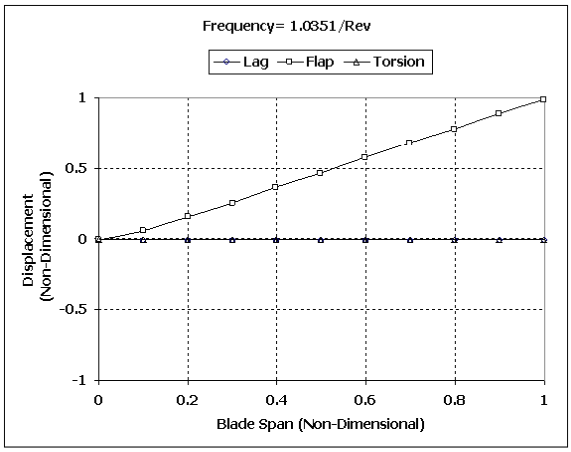

Figure 6. Schematic of the 2nd natural blade mode.

SOLUTION TECHNIQUES

The basic trim procedure used in this study is a coupled rotor-fuselage trim procedure for a helicopter in a hover and forward flight. For a given helicopter configuration, the flight condition is defined by the velocity V along the specified flight path angle γ and the turn rate $\dot{\psi}$. The straight level flight is provided as a special case with zero turn rate and fight path angle. The vector of unknowns of the trim procedure corresponds to:

$$y_{trim} = \begin{bmatrix} \theta_0 & \theta_{1c} & \theta_{1s} & \theta_{0tr} & \alpha & \beta & \\ p & q & r & \phi & \theta & \cdots & \\ \lambda_0 & \lambda_{1c} & \lambda_{1s} & v_{tr} & \cdots & & \\ q_0^1 & q_{1c}^1 & q_{1s}^1 & \cdots & q_{N_h c}^1 & q_{N_h s}^1 & \cdots \\ q_0^{Nm} & q_{1c}^{Nm} & q_{1s}^{Nm} & \cdots & q_{N_h c}^{Nm} & q_{N_h s}^{Nm} & \cdots \\ x_0^1 & x_{1c}^1 & x_{1s}^1 & \cdots & x_{M_h c}^1 & x_{M_h s}^1 & \cdots \\ x_0^{Np} & x_{1c}^{Np} & x_{1s}^{Np} & \cdots & x_{M_h c}^{Np} & x_{M_h s}^{Np} & \end{bmatrix}^T \qquad (40)$$

As noted earlier, in the current work, the modal coordinate transformation is applied to reduce the number of degrees of freedom of the main rotor blades. The modal coefficients for each flap, lag or torsion mode are expanded in a truncated Fourier series, and the coefficients of the expansions become unknowns of the trim problem. The q_0^k is the constant coefficient and q_{js}^k, q_{jc}^k are respectively the coefficients of the j-th harmonic Cosine and Sine for the k-th blade mode. The presented results in this research are obtained for two flap, two lag and two torsional modes by including the three harmonics $N_h = 3$ in the expansion of the modal coefficient.

The trim problem is defined by a set of coupled nonlinear algebraic equations that impose three-force

and three-moment equilibrium along the aircraft body fixed coordinate system axes; three kinematic relations between roll, pitch and yaw rates and turn rate; one equation imposing coordinated turn, and one kinematic condition on the flight path angle.

The unsteady aerodynamic states are also expanded in a truncated Fourier series, and hence the coefficients of the expansions are considered as unknowns of the trim problem. The x_0^k is the constant coefficient and x_{js}^k, x_{jc}^k are respectively the coefficients of the j-th harmonic Cosine and Sine for the selected k-th point per blade.

RESULTS

In this section, the transient response of an articulated rotor helicopter to step-inputs at various trim conditions has been calculated and compared with flight test data [18]. The test data used for comparison were obtained in a series of tests conducted for use in validation of the Rotorcraft Systems Integration Simulator. The trim data and selected transient-response time histories were provided to Sikorsky for use in their validation of the mathematical models. No stability augmentation was used during transient-response data runs. Analog and digital stability augmentation systems, the flight path stabilization system, and the horizontal stabilizer control system were disabled. This is a highly degraded configuration; the results are not representative of a UH-60A in normal operation. The test procedure normally consists of stabilizing in trim with one of the two redundant stability augmentation systems on; this was disabled one second before the control input. Unsatisfactory stability characteristics of the un-augmented aircraft, especially in pitch, required the pilot to initiate recovery within a few seconds of the input for reasons of instability or safety. Furthermore, because the test program was organized in order to provide standard handling qualities data, the presented results are focused on both off-axis and on-axis dynamic response. Validations are discussed in terms of the pitch, roll and yaw rate responses, which are important from the handling qualities point of view.

In all cases, trim control settings are normally obtained from the previous section for 50 knots forward flight speed, corresponding to $\mu = 0.11$ respectively. All results are taken for an altitude of 3000 feet in a standard atmosphere and a gross weight of 16000 lbf. This corresponds to a $\frac{C_T}{\sigma}$ of 0.069.

The current analysis uses six main rotor blade

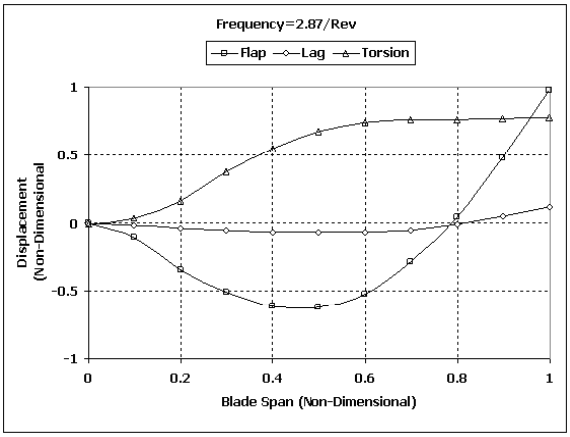

Figure 7. Schematic of the 3rd natural blade mode.

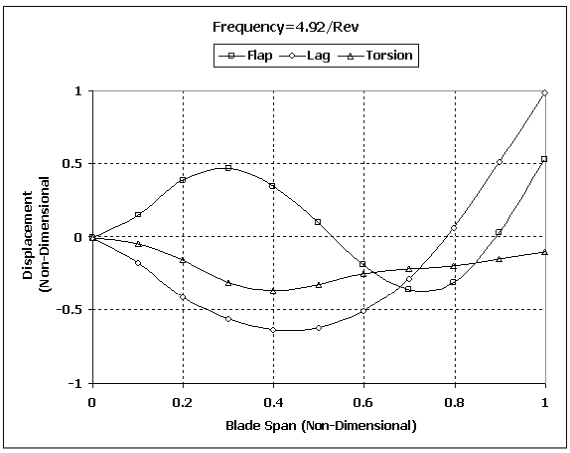

Figure 8. Schematic of the 4th natural blade mode.

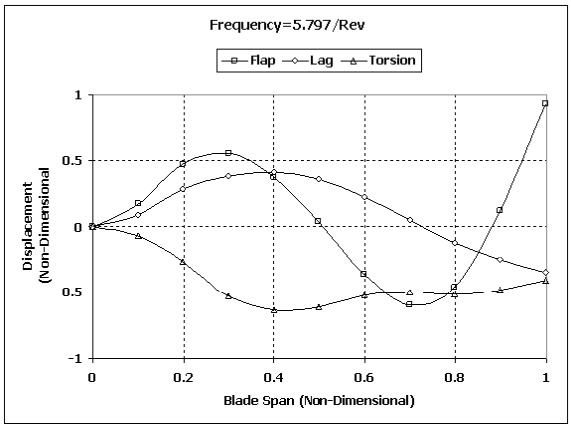

Figure 9. Schematic of the 5th natural blade mode.

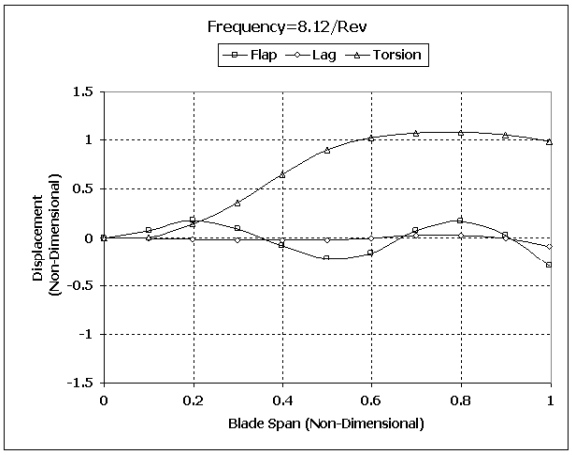

Figure 10. Schematic of the 6th natural blade mode.

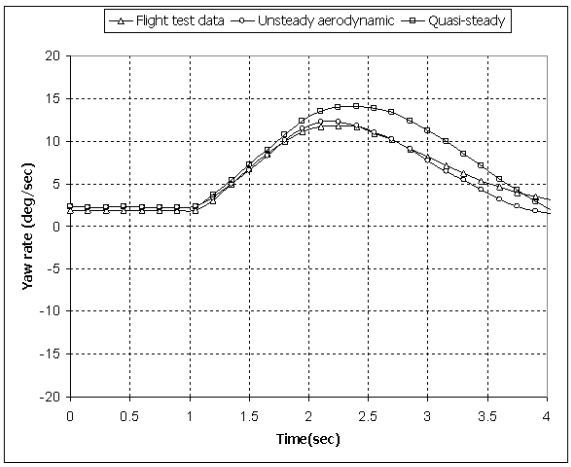

Figure 11. On-axis yaw rate response to pedal input, forward flight.

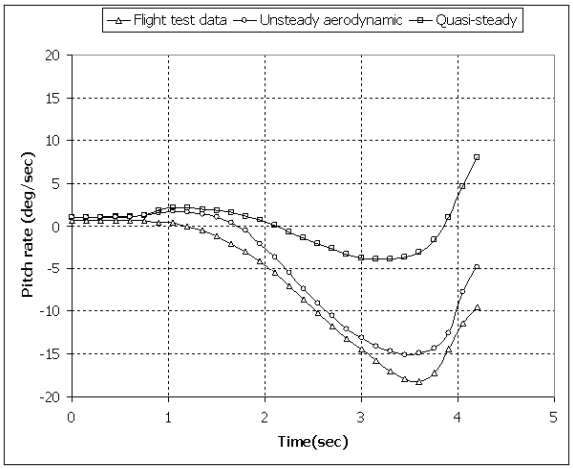

Figure 12. Off-axis pitch rate response to pedal input, forward flight.

modes to model the rotor flexibility, which include two natural flap modes, two natural lag modes, and two natural torsion modes resulting from the finite element analysis. Five finite elements are used in the calculation of these modes. The blade mass and stiffness distributions are obtained through lookup tables [15]. The natural frequencies of the modes are presented in the followed figures. This mode is calculated with the geometric pitch angle at the root of the blade set to zero and the centers of gravity and shear coincident at the quarter-chord to reduce the flap-lag and flap-torsion coupling. The presence of the large amount of structural twist,-14°, of the blade for this case have a significant influence on the coupling between the flap and lag modes. Figures 5 through 10 display the six lowest frequency natural mode shapes that are generated for five finite elements with non-uniform mass and stiffness distributions.

Figures 11 through 13 show the pitch, roll and yaw rate responses of the helicopter at 50 knots straight and level flight to 1 degree step pedal input maneuver. As shown in Figure 11, it can be seen that the maximum on-axis yaw rate response is achieved in about 2 seconds after the control input is applied. The initial acceleration is followed by a rapid growth to maximum rate 12 degrees per second when the control and damping moments are effectively in balance. The restoring moments ultimately enforce the response back to the primary equilibrium path. Although, this is predicted by both of the unsteady and the quasi steady aerodynamic modeling, the unsteady aerodynamic model shows improvement during the simulated time.

However, based on Figure 9, the predicted unsteady off-axis pitch rate response closely follows flight test data, both quantitatively and qualitatively, while the quasi-steady deviates from the actual data. The discrepancy is probably due to high damping moment which is predicted poorly by the quasi-steady modeling and is modified by applying unsteady aerodynamic within both circulatory and non-circulatory load terms.

The discrepancies observed in Figure 13 are due to both predefined non-circulatory time constants and

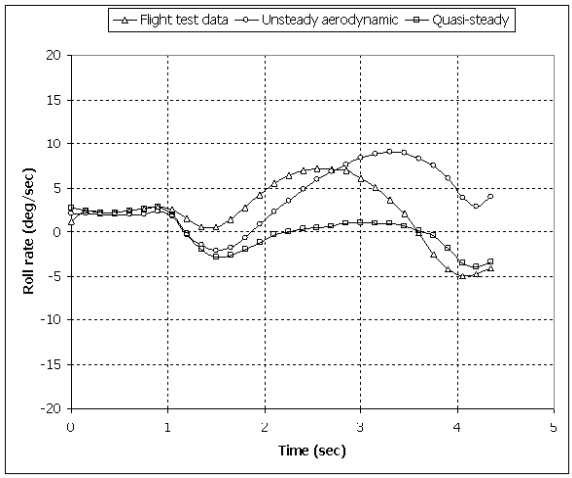

Figure 13. Off-axis roll rate response to pedal input, forward flight.

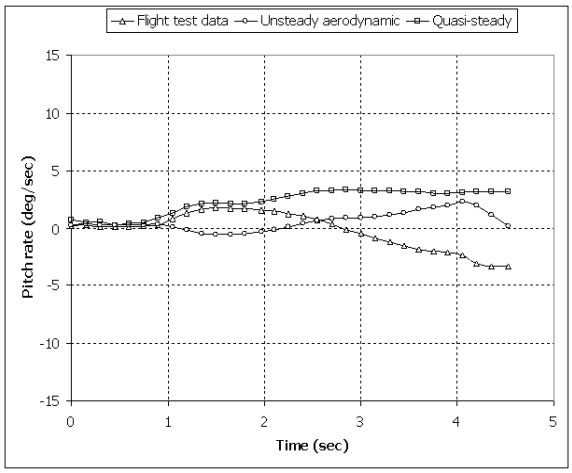

Figure 14. Off-axis pitch rate response to lateral cyclic input, forward flight.

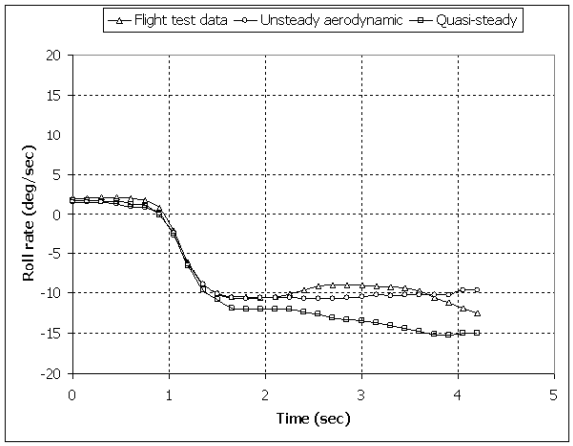

Figure 15. On-axis roll rate response to lateral cyclic input, forward flight.

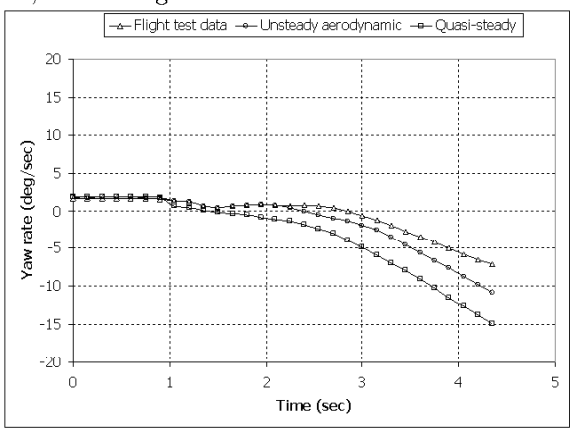

Figure 16. Off-axis yaw rate response to lateral cyclic input, forward flight.

circulatory load coefficients. The initial roll acceleration due to application of pedal displays larger roll amplitude with smaller roll damping moment in comparison with flight test data. The unsteady predicted response shows a higher accuracy compared with the quasi-steady base line model.

Figures 14 through 16 depict pitch, roll and yaw rate response due lateral cyclic stick input at 50 knots forward flight speed. As shown in Figure 14, the initial transient pitch response is first traced to a maximum rate at which the control and damping moment are being balanced. The figure shows that the pitch rate response still suffers a problem, possibly due to the restoring moment which arises from the aircraft translational acceleration. The sign of restoring moments is strongly dependent on the amount of the induced velocity variations which considerably affect the main rotor reaction.

As shown in Figure 15, the on-axis roll rate response both qualitatively and quantitatively follows the actual flight test data. This means that the unsteady indicial based approach well simulates the unsteady conditions around the main rotor which has a major contribution in the dynamic behavior of a helicopter as a whole. It can be seen that both the circulatory and non-circulatory time constants are sufficiently accurate when the prediction of an on-axis response under the action of an on-axis input is concerned. As clearly seen, the unsteady aerodynamic theory presents an improvement in comparison with what the quasi steady approach shows.

In Figure 16, a good correlation is seen when the unsteady aerodynamic model is applied for studying the yaw rate response. This is certainly because of the use of the inflow dynamic model which adds a normal velocity component to the rotor disk alone. Since, the dynamic inflow model adds the normal velocity component instead of the lateral-directional components; the off-axis response is quite close to actual flight test data both qualitatively and quantitatively. Hence, the dynamic inflow model rather than the unsteady aerodynamic model is recognized as a principal source of error.

CONCLUSIONS

A practical implementation of the unsteady aerodynamic loads has been presented through the comprehensive flight dynamic simulation program. This time domain unsteady aerodynamic formulation, coupled with a compatible dynamic inflow model, finite element discritization and a numerical solution technique, provides an improvement in the dynamic response prediction of helicopters.

The presented formulation is considered as an intermediate method between the steady state linearized incompressible and the more comprehensive unsteady aerodynamic formulation based on computational fluid dynamics methods CFD. The main advantage of this model is that the unsteadiness around the helicopter dynamics can be explicitly modeled in time domain through a set of ordinary differential equations without any constraint on a solution algorithm. Response improvement is achieved by considering the circulatory, the non-circulatory terms and the compressible flow assumption which are applied to arbitrary points on the span wise location of blades. Both the on-axis and off-axis response predictions of the simulated model are in good agreement with available flight test data. Thus, this model can be used as a tool for better determination of helicopter handling qualities. Consequently, the movement from the quasi-steady to the unsteady aerodynamics is a logical trend for improvement of the dynamic response prediction of helicopters.

ACKNOWLEDGEMENT

The authors wish to express their appreciation to the Sharif University of Technology for supporting this research.

REFERENCES

1. Rosen, A., and Isser, A., "A Model of the Unsteady Aerodynamics of a Hovering Helicopter Rotor that Includes Variations of the Wake Geometry", *Journal of the American Helicopter Society*, **40**, PP 6-16(1995).
2. Rosen, A., and Isser, A., "A New Model of Rotor Dynamics during Pitch and Roll of a Hovering Helicopter", *Journal of the American Helicopter Society*, **40**, PP 17-28(1995).
3. Keller, J. D., "An Investigation of Helicopter Dynamic Coupling Using an Analytical Model", *Journal of the American Helicopter Society*, PP 322-330(1996).
4. Arnold, U. T. P., Keller, J. D., Curtiss, H. C., J., and Reichert, G., "The Effect of Inflow Models on the Predicted Response of Helicopters", *Journal of the American Helicopter Society*, **43**, PP 25-36(1998).
5. Basset, P. M., "Modeling of the Dynamic Inflow on the Main Rotor and the Tail Components in Helicopter Flight Mechanics", *Proceedings of the 22nd European Rotorcraft Forum*, Brighton, UK., (1996).
6. Von Grunhagen, W., "Dynamic Inflow Modeling for Helicopter Rotors and Its Influence on the Prediction of Cross-Couplings", *American Helicopter Society 2nd International Aeromechanics Specialists Conference*, Bridgeport, CT., (1995).
7. Mansur, H. M. and Tischler, M. B., "An Empirical Correction Method for Improving Off-Axis Response Prediction in Component Type Flight Mechanics Helicopter Model", *AGARD Flight Vehicle Integration Panel on Advances in Rotorcraft Technology*, Ottawa, Canada, (1996).
8. Ribera, M., and Celi, R., "Simulation Modeling of Unsteady Maneuvers Using a Time Accurate Free Wake", *American Helicopter Society 60th Annual Forum Proceedings*, Baltimore, (2004).
9. Ribera, M., and Celi, R., "Simulation Modeling in Steady Turning Flight with Refined Aerodynamics", *Proceedings of the 31st European Rotorcraft Forum*, Firenze, Italy, (2005).
10. Ribera, M., and Celi, R., "Simulation Modeling in Climbing and Descending Flight with Refined Aerodynamics", *Proceedings of the 62nd Annual Forum of the American Helicopter Society*, Phoenix, (2007).
11. Lovera, M., Colaneri, P., Malpica, C., and Celi, R., "Discrete-Time, Closed-Loop Aeromechanical Stability Analysis of Helicopters with Higher Harmonic Control", *Journal of Guidance, Control, and Dynamics*, **30**, (2007).
12. Theodore, C. and Celi, R., "Prediction of the Off-Axis Response to Cyclic Pitch Using a Maneuvering Free Wake Model", *25th European Rotorcraft Forums*, Rome, Italy, (1999).
13. Celi, R., "State-Space Representation of Vortex Wakes by the Method of Lines", *Journal of the American Helicopter Society*, **50**, PP 195-205(2005).
14. Ribera, M., and Celi, R., "Time Marching Simulation Modeling in Axial Descending Flight Through the Vortex Ring State", *Proceedings of the 63rd Annual Forum of the American Helicopter Society*, Virginia Beach, (2007).
15. Shahmiri, F. and Saghafi, F., "Improvement of Dynamic Response Prediction of Helicopters", *Journal of Aircraft Engineering and Aerospace Technology*, **79**, PP 579-592(2007).
16. Leishman, J. G. and Nguyen, K. Q., "State-Space Representation of Unsteady Airfoil Behavior", *AIAA journal*, **28**, PP 836-844(1990).
17. C. de Boor, *A Practical Guide to Splines*, Springer-Verlag, (1978).
18. Ballin, M.G., *Validation of a Real-Time Engineering Simulation of the UH-60A Helicopter*, NASA TM-88360, (1981).